ANALYSIS OF ELECTRON MULTIPACTING IN COAXIAL LINES WITH TRAVELING AND MIXED WAVES

Pasi Ylä-Oijala
Rolf Nevanlinna Institute
University of Helsinki, Finland

November 5, 1997

Abstract

In this report the electron multipacting is analyzed in coaxial lines for a time–harmonic wave which is either a pure one–way traveling or a mixed wave, i.e., a combination of a standing wave and a traveling one. Two families of multipacting are found when the wave is partially reflected. In the case of one–way traveling wave these families are merged together and the multipacting electrons are traveling along with the wave. Thus, in the traveling wave operation, multipacting may occur on the entire line. On the other hand, in the mixed wave operation multipacting is due to certain fixed points in the phase space and the two MP families have essentially different behavior. We give simple scaling laws for the multipacting power levels, when the wave is switched from the standing wave to a traveling one (and vice versa). Also the previously found scaling laws for the standing wave multipacting power levels with respect to the diameter, frequency and impedance of the line are found to be valid for the traveling and mixed waves. The numerical computations of this report were carried out during the joint project of Rolf Nevanlinna Institute and Deutsches Elektronen–Synchrotron (DESY).

1 Introduction

Electron multipacting (MP) is one of the biggest problems in coaxial input couplers. The phenomenon starts if certain resonant conditions for electron trajectories are fulfilled and if the impacted surface has a secondary yield larger than one. In appropriate conditions, the number of electrons may increase exponentially, leading to remarkable power losses, gassing of the surface and heating of the walls. The resonance conditions for MP are

(1) An electron emitted from the cavity wall is driven by the EM fields and returns back after an integer number of rf cycles to the same point of the cavity wall.

(2) The impacting electron produces more than one secondary electron.

In the previous report [2] we developed computational methods to analyze electron MP in rf structures. The methods were applied numerically to analyze MP in coaxial lines with the standing waves (SW). We were able to recognize those rf power levels at which MP may

occur and thereafter, to locate and identify MP processes of different type. We showed that in the SW case MP appears always close to the maximum of the electric field, where the magnetic field is close to zero and hence, the repelling force $\vec{v} \times \vec{B}$ due to the magnetic field is minimal. This kind of MP, which is predominantly due to the electric field only, is called *electric multipacting* (EMP). Further, we recognized two different dominant MP types. First, there are one–point MP processes of different order on the outer conductor of the line. Secondly, there are two–point processes from the outer conductor to the inner one and back. Furthermore, in straight coaxial lines with the SW operation we found certain simple scaling laws for the MP power bands with respect to the field frequency (f), the diameter of the line (d) [2] and the impedance of the line (Z) [3]. The scaling laws are

$$P_{\text{one-point}} \sim (f\,d)^4\,Z, \quad P_{\text{two-point}} \sim (f\,d)^4\,Z^2, \tag{3}$$

In many cases it is important to understand the behavior of the MP power levels when the field is switched from SW to the traveling wave (TW), i.e., the reflected wave vanishes. Since the standing wave case is systemically considered in the previous report [2], here we focus the discussion to the traveling waves and to a combination of SW and TW, so called mixed waves (MW), or partially reflected waves. In these cases the numerical analysis of MP is performed with the methods described in [2]. The main idea of the method is briefly reviewed here in Section 2. In the numerical computations we have considered the 1.3 GHz, 50 Ω coaxial line, and the outer diameter of the line is 40 mm. The main results of the research will be also presented in the forthcoming paper [4].

2 Methods to analyze multipacting

In this section we give a short review of the computational methods used to analyze MP in rf structures. For more details we refer to [2] (and [4]).

First, we send at a fixed incident power a sufficiently large number of electrons from different points of the wall of the cavity in different field phases. The initial velocity being a few eV and perpendicular to the wall.[1] Then the electron trajectories are computed and the place of the first impact on the wall together with the impact energy and corresponding field phase are recognized. If the field phase is such that possible secondary electrons are able to leave the wall, the trajectory calculation is continued. Let us denote $X = \partial\Omega \times [0, 2\pi[$, where $\partial\Omega$ denotes the wall of the cavity. Here X is called the *phase space*. The part of X from where the electrons are able to leave the wall, due to an appropriate direction of the field, is called a *bright set*. The remaining part of X, from where the electrons are not able to leave the wall is called a *shadow set*. After a given number of impacts (usually 30 impacts are calculated), the number of electrons in the bright set, i.e., the number of electrons able to produce secondary electrons, is counted. Depending on whether the secondary yield function is taken into account, we call this total number of electrons as the *counter function* (no secondary yield included), denoted by $c_n(P)$ or the *enhanced counter function* (secondary yield included), denoted by $e_n(P)$. We repeat the trajectory calculations with several fixed power values. Obviously, if the counter function $c_n(P)$ is large for some power P, the geometry and the dynamics create trajectories that may cause MP. Further, the enhanced counter function $e_n(P)$ tells whether the secondary yield is large enough for MP.

[1] In reality the orientation of the initial velocity varies, but because the energy of the field inside the line is much higher than a few eV, the variation of the initial velocity is not significant.

Once the possible MP power levels are recognized, we need to locate the different MP processes in the phase space X. For this purpose we have defined the following *distance function*

$$d_n(p) = \sqrt{|x_0 - x_n|^2 + \gamma |e^{i\varphi_0} - e^{i\varphi_n}|^2}, \tag{4}$$

where γ is a properly chosen scaling factor (here $\gamma = \lambda/(2\pi)$), $p = (x_0, \varphi_0)$ is the initial point and (x_n, φ_n) is the impact point after n impacts. Obviously, the minima of the function d_n point out the starting points and phases of those resonant trajectories that survive n impacts and are able to multipact.

Figure 1 shows the plot of the relative electron counter $c_{30}(P)/c_0(P)$ in the SW operation when the computation is restricted to the maximum of the electric field. Multiplying by 100 % the values on the vertical axis tells how many percent of initially launched electrons are still in the bright set after 30 impacts. The orders of the most dominant processes are indicated in the plot. The process marked by "mix" is a combination of a two–point process of order one and an one–point process of order two.

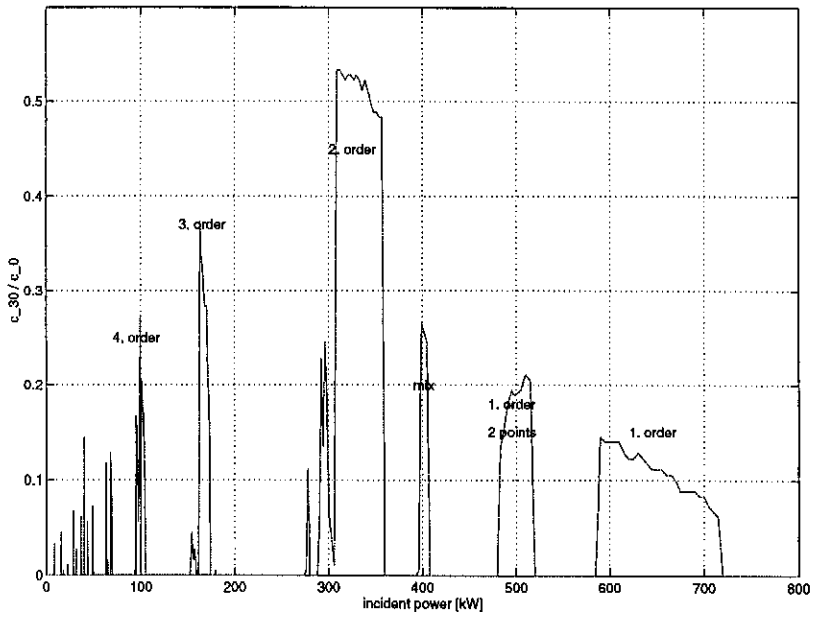

Figure 1. Relative electron counter after 30 impacts in the SW operation.

Figure 2 gives the corresponding relative enhanced counter function in the base 10 logarithmic scale. MP occurs when the enhanced counter function is greater than one, i.e., the number of electrons is increased. Therefore, all peaks above the solid line correspond to MP processes of different type and order, and the corresponding power bands can be read from the horizontal axis. In this report we use the secondary yield function given in [2], which is a typical function for a niobium surface. The function is originally presented in [1].

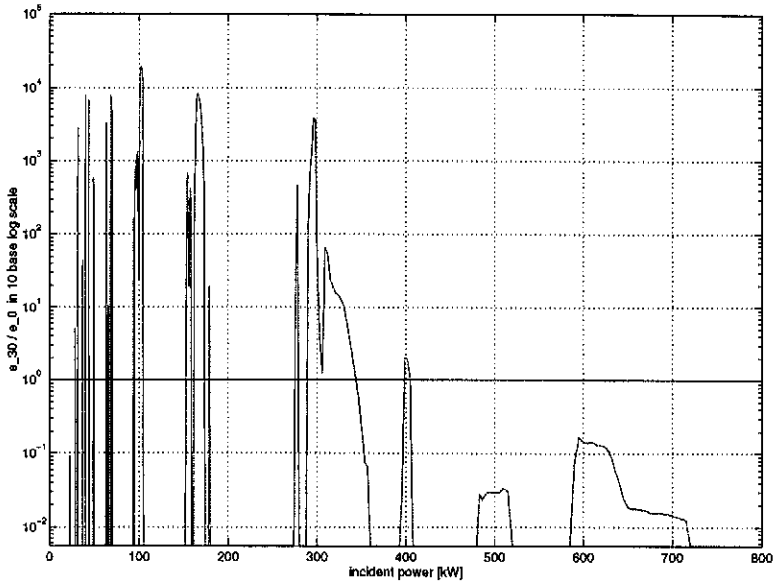

Figure 2. Relative enhanced electron counter after 30 impacts in the SW operation.

3 Traveling waves

First the pure TW operation is considered. We consider time–harmonic waves with the time factor $e^{-i\omega t}$. Let a and b denote the inner and outer radii of the coaxial line, and let f denote the frequency and U denote the voltage drop between the inner and outer conductor. Then the TEM–mode fields in TW operation are given by the formulae

$$\begin{aligned} \vec{E}_{TW}(x,\varphi) &= \frac{U}{r\log(b/a)}(\cos(kz-\varphi))\,\vec{e}_r, \\ \vec{B}_{TW}(x,\varphi) &= \frac{U}{cr\log(b/a)}(\cos(kz-\varphi))\,\vec{e}_\phi, \end{aligned}$$

with $c = 1/\sqrt{\varepsilon_0\mu_0}$ and $k = \omega/c$. Here (r,ϕ,z) is the representation of the field point x in cylindrical coordinates, $\varphi = \omega t$ is the phase of the field and t is time. The average *incident power* flow P of the (TW) electromagnetic field is related to the voltage U through the formula

$$P = \frac{U^2}{2\,Z}, \quad Z = \frac{\eta_0}{2\pi}\log\frac{b}{a}. \tag{5}$$

where Z is the line impedance and η_0 is the wave impedance in vacuum.

To find possible MP power levels, we compute the counter function $c_n(P)$ initiating electrons from both the inner and outer conductors of the line in different field phases. The electrons initiated from the inner conductor are, however, drifted to the similar trajectories as the electrons initiated from the outer conductor. Similar property was observed in the SW operation, too. Thus, the one–point processes appear on the outer conductor only. Figure 3 shows the relative electron counter function after 30 impacts. Comparing Figures 1 and 3 we observe that the counter functions in the SW and TW cases are almost identical.

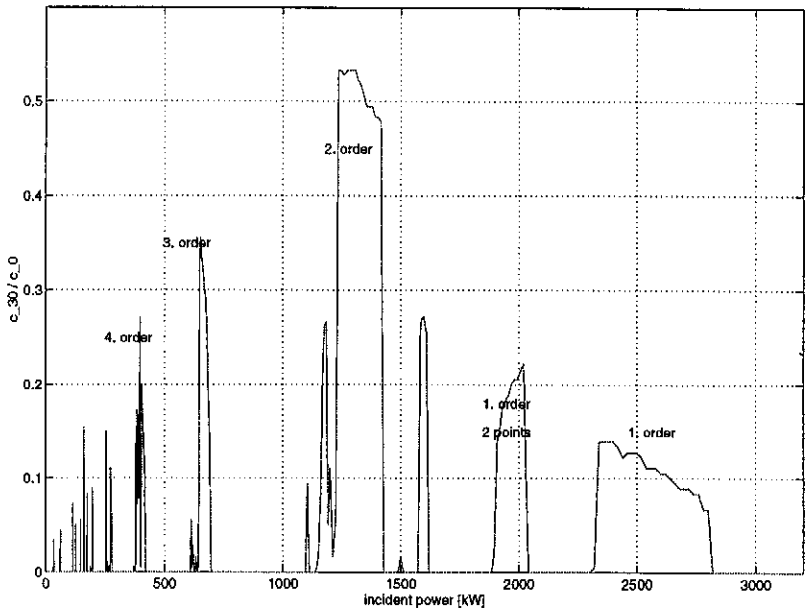

Figure 3. Relative electron counter after 30 impacts in the TW operation.

Furthermore, a closer analysis of electron trajectories shows that processes of similar type can be identified in both operations. In the TW operation the MP power bands appear at four times higher power values than the corresponding power bands in the SW operation. Thus, we get a simple rule for the MP power bands of different order

$$P_{TW} = 4\,P_{SW}. \tag{6}$$

Heuristically, the physical explanation to this phenomenon is pretty simple. The peak voltage in the SW operation is twice the peak voltage of the TW, which means four times in the terms of the incident power.

However, the electron counter function tells only the number of surviving electrons, i.e., it shows the rf power levels at which the geometry and electron dynamics are suitable for stationary trajectories. The actual number of secondary electrons depends on the impact energy and the material properties of the impacted surface. Figure 4 shows the square root of the average impact energy in eV of those electrons which are still in the bright set after 30 impacts. Between the solid lines the used secondary yield is larger than one, and the maximum yield 1.5 is reached when the impact energy is about 400 eV (denoted by a dashed line). A closer analysis of the impact energy shows that only the processes of order 2 - 9 are able to multipact, because then the impact energy is in the suitable range. This is clearly demonstrated in Figure 5, where we have plotted the base 10 logarithmic of the relative enhanced electron counter function after 30 impacts. The counter functions in Figures 2 and 5 (the SW and TW cases) are still surprisingly identical. Thus, we may conclude that the average impact energy and therefore, the secondary yield of the corresponding processes in the SW and TW operations are of the same size.

Although processes of similar type can be identified in the SW and TW operations, the trajectories of the MP electrons are not identical. Figure 6 shows the MP trajectories in the TW operation, when the incident power is chosen to correspond to the one–point process of

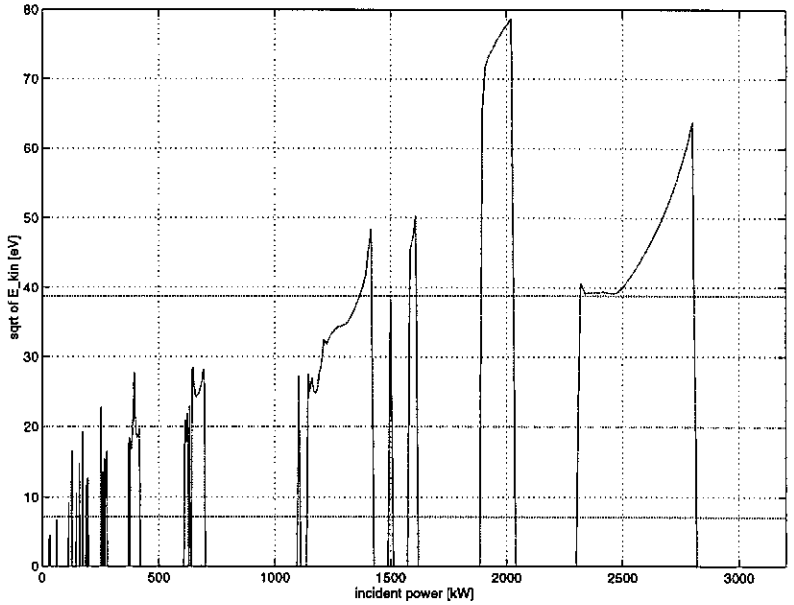

Figure 4. Average impact energy in 30 impacts in the TW operation.

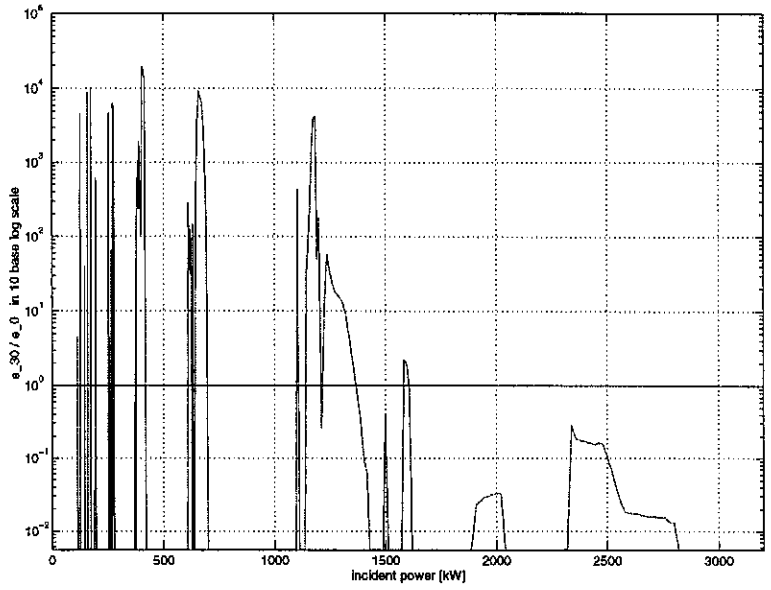

Figure 5. Relative enhanced electron counter after 30 impacts in TW operation.

order one ($P = 2600$ kW) and two ($P = 1300$ kW), and the two–point process of order one ($P = 1900$ kW). Here we have plotted 5 impacts and the initial points are on the left (at $z = 0$ or at time $= 0$). An important feature is that the electrons are traveling along with the wave, from left to right, as the wave form moves. Furthermore, the electrons are taking constant steps between wall impacts, as Figure 6 shows, and they are moving to the same direction as the wave propagates. However, this traveling phenomenon is rather slow, only about 1 mm or less between the wall impacts. Further, the traveling in the axial direction is very small compared with the movement in the radial direction. In this particular geometry, the ratio of the axial and radial move of the MP electrons is roughly 1/10. Due to this traveling phenomenon, stationary MP trajectories may occur only if *the field form stays similar on each impact.* In addition, MP may now appear on the entire line, in contrast to SW, where MP may appear only on a discrete set of points, namely at the maxima of the electric field.

Figure 7 gives the traveling velocity of the MP electrons in mm, i.e., the distance between adjacent wall impacts, as a function of the order of the one–point process for the 40 mm, 1.3 GHz, 50 Ω line. The velocity seems to decrease roughly inversely proportionally to $(n + 1)$ where n is the order of the process. Next the effect of varying the dimensions of the line and the frequency of the field to the traveling velocity was checked. In Figure 8 the traveling velocity of a one–point process of order one is plotted when the outer diameter of the line varies (the picture on the top), when the frequency of the field varies (the picture in the middle) and when the impedance of the line varies (the last picture), respectively. While varying one variable the others are fixed as $d = 40$ mm, $f = 1.3$ GHz and $Z = 50\,\Omega$. Figure 8 shows that the traveling velocity of the MP electrons depends quadratically on the outer diameter of the line, linearly on the frequency of the field and it is totally independent of the variation of the impedance of the line. The results of Figures 7 and 8 can be summarized by the following scaling law

$$v_{\text{traveling}} \sim \frac{d^2 f}{1+n}. \tag{7}$$

The knowledge of the traveling velocity might give a hint, for example, how dense grooving should be used to suppress MP of certain order in the given geometry with the TW operation.

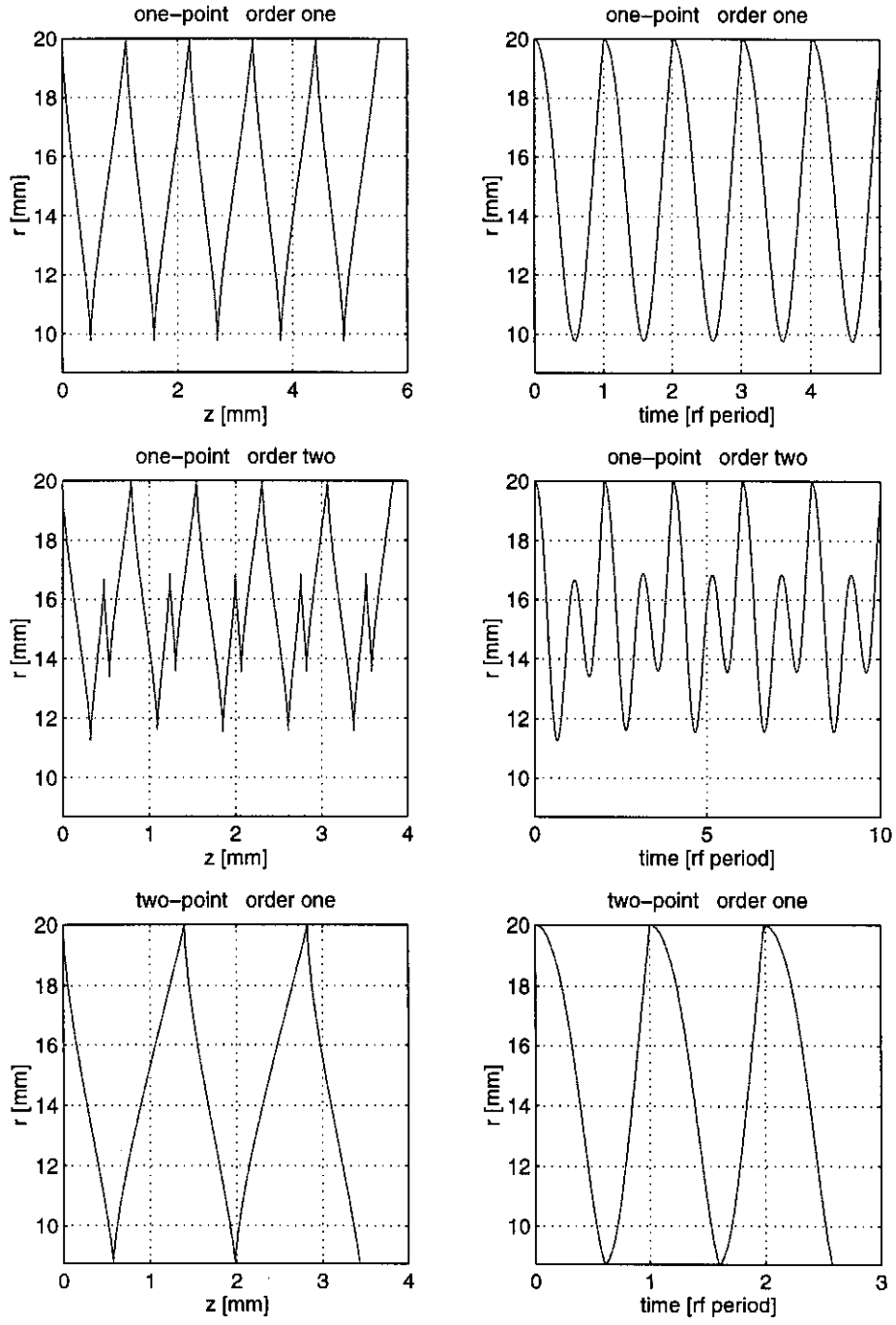

Figure 6. Electron trajectories due to the one–point processes of order one and two, and two–point process of order one. The pictures on the left hand side give the trajectories in r/z coordinates and the pictures on the right hand side give the trajectories in $r/time$ coordinates. The upper and lower borders of the pictures correspond to the outer and inner conductors of the line.

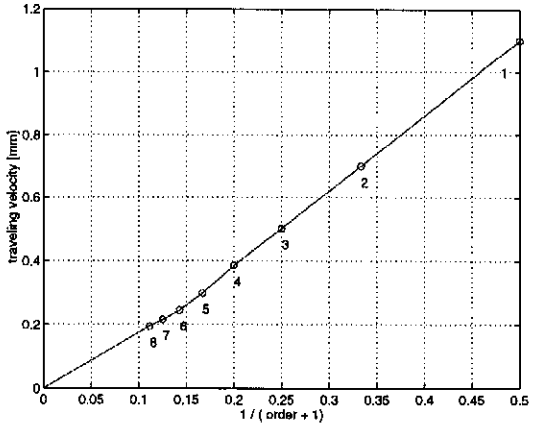

Figure 7. Traveling velocity of the multipacting electrons in mm as a function of the order of the (one–point) process.

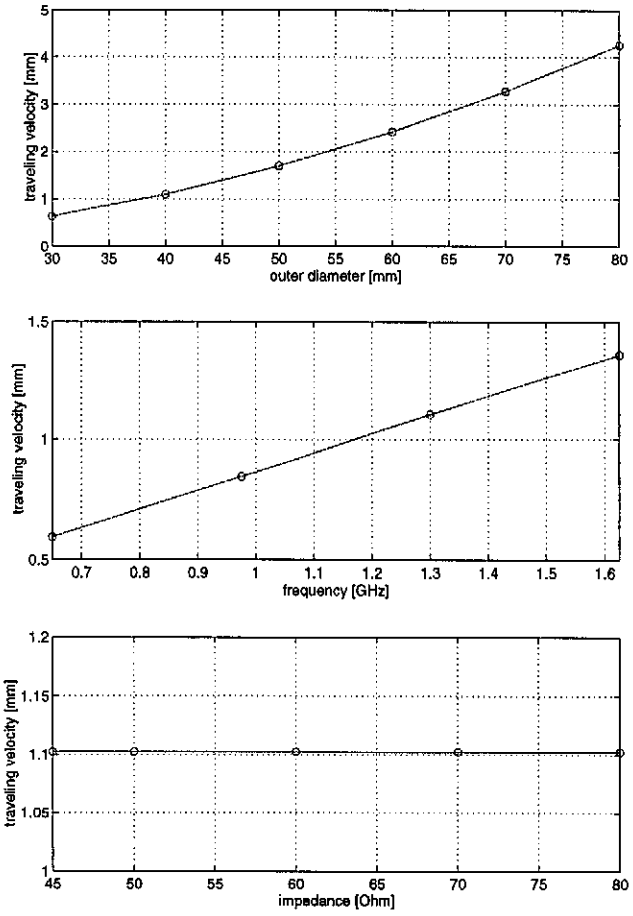

Figure 8. Traveling velocity of the multipacting electrons in mm as a function of the outer diameter of the line (the top frame), frequency of the field (the middle frame) and impedance of the line (the bottom frame).

4 Mixed waves

Next consider a combination of a superposition of the SW and TW fields

$$\begin{aligned} \vec{E}_R &= R\,\vec{E}_{SW} + (1-R)\,\vec{E}_{TW}, \\ \vec{B}_R &= R\,\vec{B}_{SW} + (1-R)\,\vec{B}_{TW}, \end{aligned}$$

where R, $0 \leq R \leq 1$, is the *reflection coefficient.* Obviously, if $R = 1$ we have the SW fields (total reflection) and if $R = 0$ we have the TW fields (no reflection), respectively. With the other values of R, the wave is partially reflected and called a *mixed wave.* The forward power of a mixed electromagnetic wave is given by

$$P_R = \frac{U_R^2}{2\,Z}\frac{1}{(1+R)^2},$$

where U_R is the peak voltage of a MW.

To have a complete picture, we need two dimensional counter functions. Figure 9 shows a gray scale plot of the base 10 logarithmic of the relative enhanced counter function after 30 impacts, as a function of the incident power (in the horizontal axis) and the reflection coefficient (in the vertical axis). All positive values of the counter function correspond to the MP processes of different type and order. The zero–line or MP–line is indicated in the plot. At the bottom we have the TW power bands and at the top we have the SW power bands. The orders of the most prominent processes are marked to the plot. The white areas correspond to such combinations of the incident power and reflection coefficient where all electrons are drifted to the shadow set before 30 impacts.

Let us then study closer what happens when the TW field is switched to the SW field. We observe the following interesting features. The TW MP bands start to split into two different bands when R is increased from the minimum value $R = 0$. As R is increased to the maximum value $R = 1$, one of these bands coincide with the EMP band of the corresponding type of SW. Therefore, the SW and TW MP bands of similar type and order are related through the wave transformation from TW to SW and vice versa. The trajectory calculations show that these bands correspond to such processes which appear close to the maximum of the SW electric field. Thus, we may recognize EMP in the MW operation too. The other bands behave differently. They shift very quickly to very high power regions as R increases. The increasing seems to be at least exponential with respect to R. Further, the processes due to these bands are found to appear close to the maximum of the SW magnetic field, and thus, they are called as a (coaxial) *magnetic multipacting* (MMP). Figure 9 shows also that the secondary yield of the EMP and MMP processes of the same type and order are roughly of the same size.

Furthermore, Figure 9 suggests that the higher order EMP bands (order greater than one) disappear when the wave is partially reflected. These bands seem to appear only when the wave form is close to the SW or TW. This phenomenon is, however, only due to the discretization. As the computations below show, the EMP processes turn out to be repelling in the axial direction. Therefore, the scan of MP power levels must be performed with a very dense grid in the axial direction in order to recognize all possible MP processes. The used grid here has been too course. Using a finer grid we are able to locate the missing processes.

To summarize the situation we note that in the pure TW operation, the MP processes are of mixed nature where the EMP and MMP processes are merged together. When R is increased

from 0, the processes of different nature split into two EMP and MMP processes. The dependence of the EMP power bands on the reflection coefficient can be described by the following rule

$$P_R^{EMP} \sim \frac{1}{(1+R)^2} P_{TW} = \frac{4}{(1+R)^2} P_{SW}. \tag{8}$$

A heuristic physical explanation for this rule is similar as for the rule relating the SW and TW operations. For given R, the peak voltage is $(1+R)$ times the corresponding peak voltage of TW.

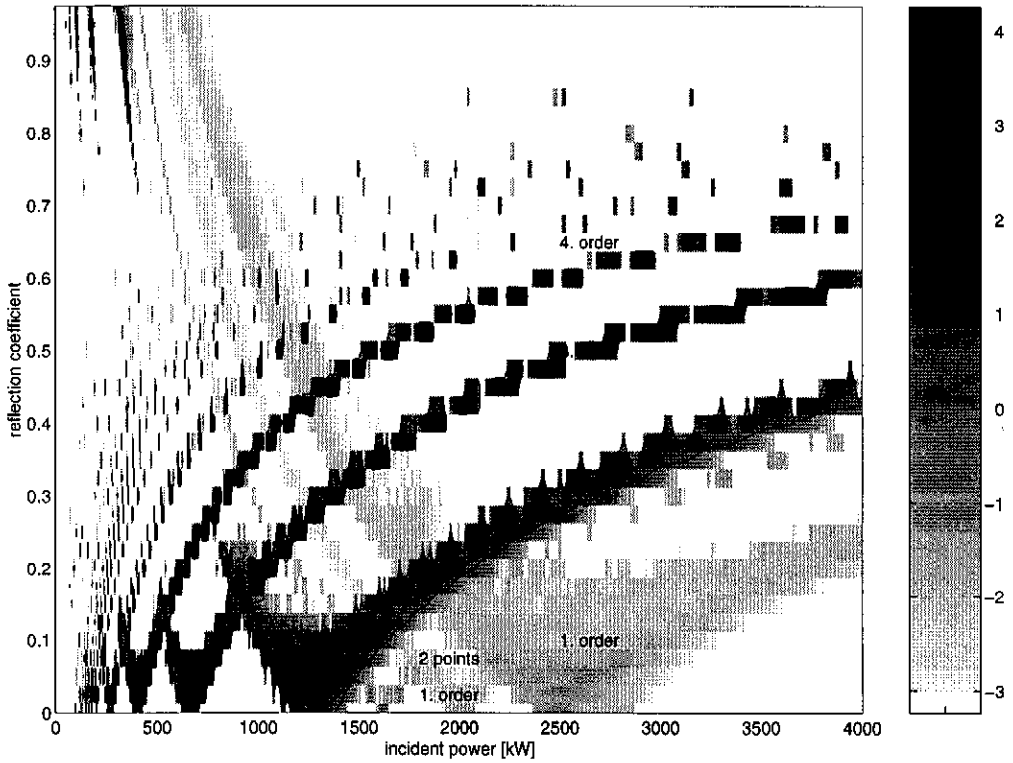

Figure 9. The gray scale plot of the base 10 logarithmic of the enhanced electron counter after 30 impacts as a function of the incident power in kW and reflection coefficient.

The drift of the MMP bands to higher incident powers when R increases can be explained qualitatively as follows. In the TEM–mode, the purely azimuthal magnetic field cannot accelerate the electrons in the radial direction and thus, cannot generate MP alone. In the TW operation, the maximum of the electric and magnetic fields coincide, and with appropriate incident powers, a suitable balance for MP can be reached. When the reflection coefficient is increased, the phase difference of the fields increases and finally in the SW operation the fields are in the opposite phases. Hence, larger and larger electric fields and thus incident powers are needed to create the needed balance for MP at the maxima of the magnetic fields. This explains also why we have not found any MMP at SW, since the incident power should be infinite then. However, we have not found any simple scaling law for the MMP power bands.

Next the EMP processes are more carefully located in the phase space when the wave is partially reflected. Figure 10 displays the distance function due to the one–point EMP process of order one when R = 1.0, 0.75, 0.5, 0.25, 0.2 and 0.1. The shaded areas give the initial

points of those trajectories which are still in the bright set after 30 impacts and therefore, able to multipact. In the horizontal axis is the z coordinate in the terms of the wave length λ, the maximum of the SW electric field being at $\lambda/4$, i.e., in the middle of the pictures. Here $\lambda = 230.6$ mm. In the first picture on the top–left, $R = 1$, i.e., the SW case, the shaded area is centered around $z = \lambda/4$ and $\varphi = 60$ degrees, i.e., close to the maximum of the electric field. When the reflection coefficient decreases, the shaded area starts to shift to the down–left and at the same time the area is becoming wider. Until in the pure TW case (not presented here), the area is spread as a band though the entire phase space. This agrees with the observation that in the TW operation MP may occur on the entire line.

Figure 11 displays the corresponding trajectories when the electrons are initiated close to the darkest spots of Figure 10. Figure 11 shows that EMP is related to certain fixed points in the phase space, in other words, electron trajectories starting from a certain location in the phase space return back after an integer number of rf cycles to the initial point. The only exception is found when $R = 0.1$. Then the traveling part of the wave is dominant and no fixed point is possible to locate, i.e., the electrons are slowly traveling along with the wave. Note that the one–point processes still appear on the outer conductor.

The MMP processes behave differently. Figures 12 and 13 display the distance function and electron trajectories due to the one–point MMP process of order three, when $R =$ 0.05, 0.1, 0.2, 0.3, 0.4 and 0.5. Now the shaded MP area stays in place as R varies, but the darkest spot, i.e., the *fixed point*, is shifting to the down–left as R decreases. Furthermore, the dark MP area is rotating counter clockwise and it is becoming smaller as R increases. The centers of the shaded areas are close to the maximum of the SW magnetic field ($z = \lambda/2$) when $\varphi = 150$ degrees.

Figure 13 gives the trajectories when the electrons are initiated close to the darkest spots of Figure 12. The pictures show that also the MMP processes are due to certain fixed points in the phase space. Now it is possible to locate a fixed point even when R is as small as 0.05.

The conclusion is the following. When the wave is partially reflected, there are certain locations in the phase space where the opposite drifting forces due the SW and TW parts of the magnetic field compensate each other and allow stationary trajectories. These locations, i.e., fixed points, are clearly visible in Figures 10 and 12 as the darkest spots and they depend on the reflection coefficient.

Figures 14 and 15 demonstrate the major difference of the EMP and MMP processes of the same type. In Figure 14 the distance functions of the one–point EMP (on the left) and MMP (on the right) processes of order one are plotted when $n = 10$, 30 and 50, and $R = 0.25$. Let us first study the pictures on the left, i.e., the EMP case. When n (number of impacts) is increased, the shaded area is becoming narrower in the axial direction, but stays in place after a few impacts in the phase direction. This suggests that the *EMP processes are repelling in the axial direction but attractive in the phase direction.* A further analysis of electron trajectories shows that this is the case, (see Figure 15). An explanation to this phenomenon is rather obvious. As in Section 3 was shown, the TW part of the field drives electrons to the one direction only. Therefore, at the maximum of the SW electric field the repelling force due to the SW magnetic field, yields to a repelling fixed point in the axial direction. On the pictures on the right, on the other hand, the size of the dark area stays fixed after a few impacts as n increases. This suggests that the *MMP processes are attractive in both directions.* A closer analysis of electron trajectories shows a validity of this suggestion, (see Figure 15). A

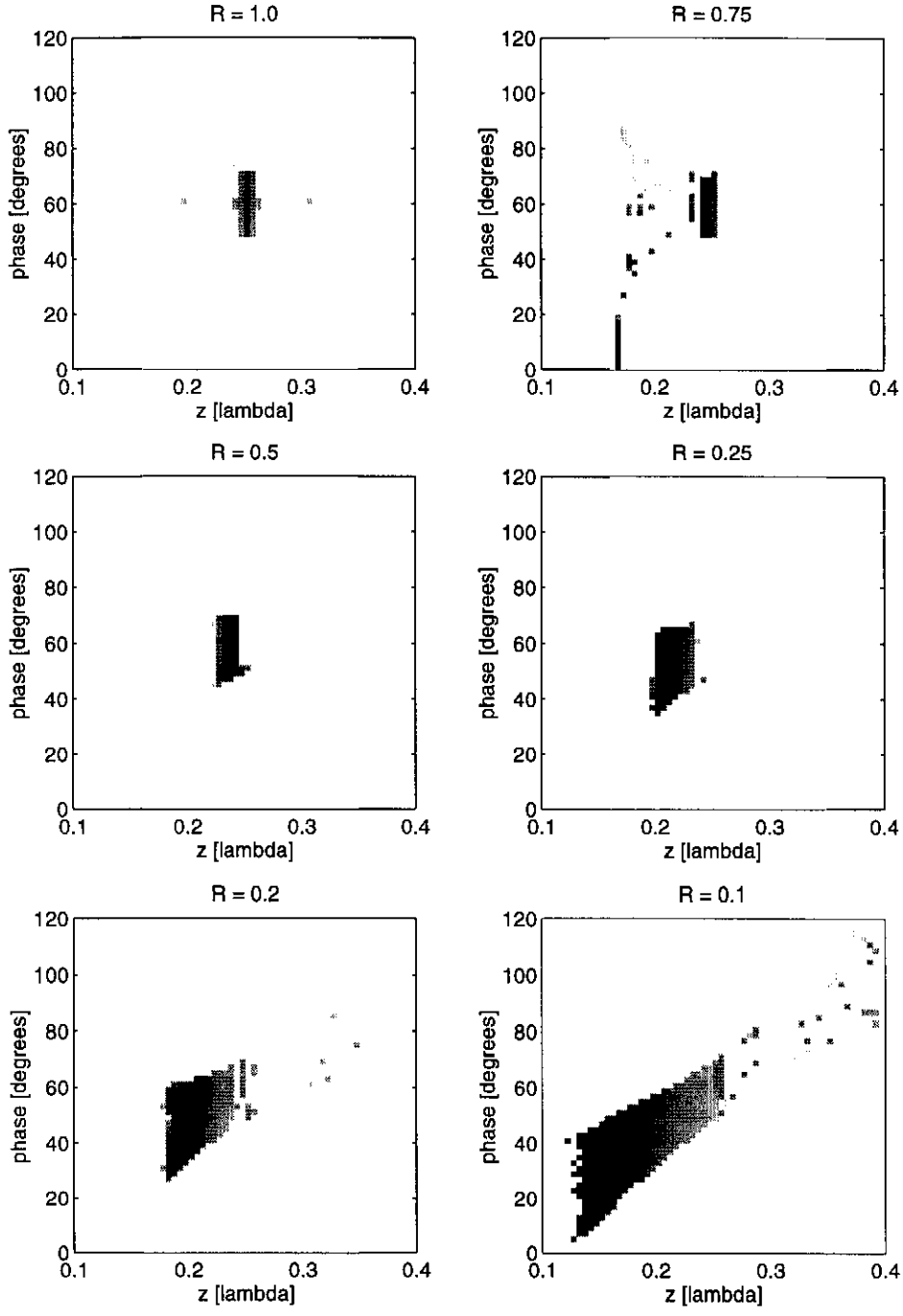

Figure 10. Distance functions due to the one–point EMP process order one when $R = 1.0,\ 0.75,\ 0.5,\ 0.25,\ 0.2$ and 0.1. The frames of the pictures correspond to the SW case.

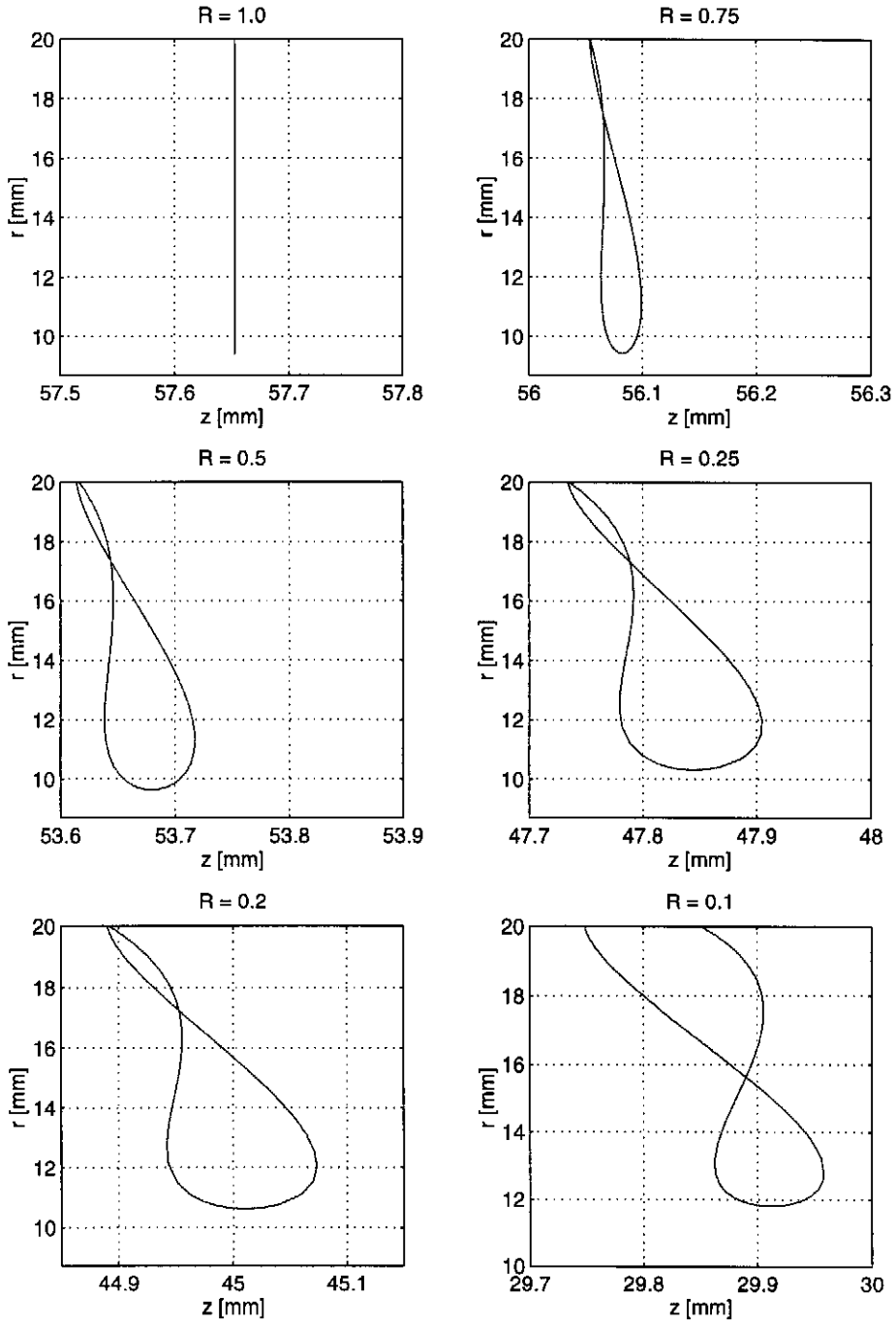

Figure 11. Electron trajectories of the one–point EMP process of order one when $R = 1.0$, 0.75, 0.5, 0.25, 0.2 and 0.1. The upper and lower borders of the pictures correspond to the outer and inner conductors of the line and the dimensions are given in mm. Note that the trajectories are predominantly radial (the axices have different scaling).

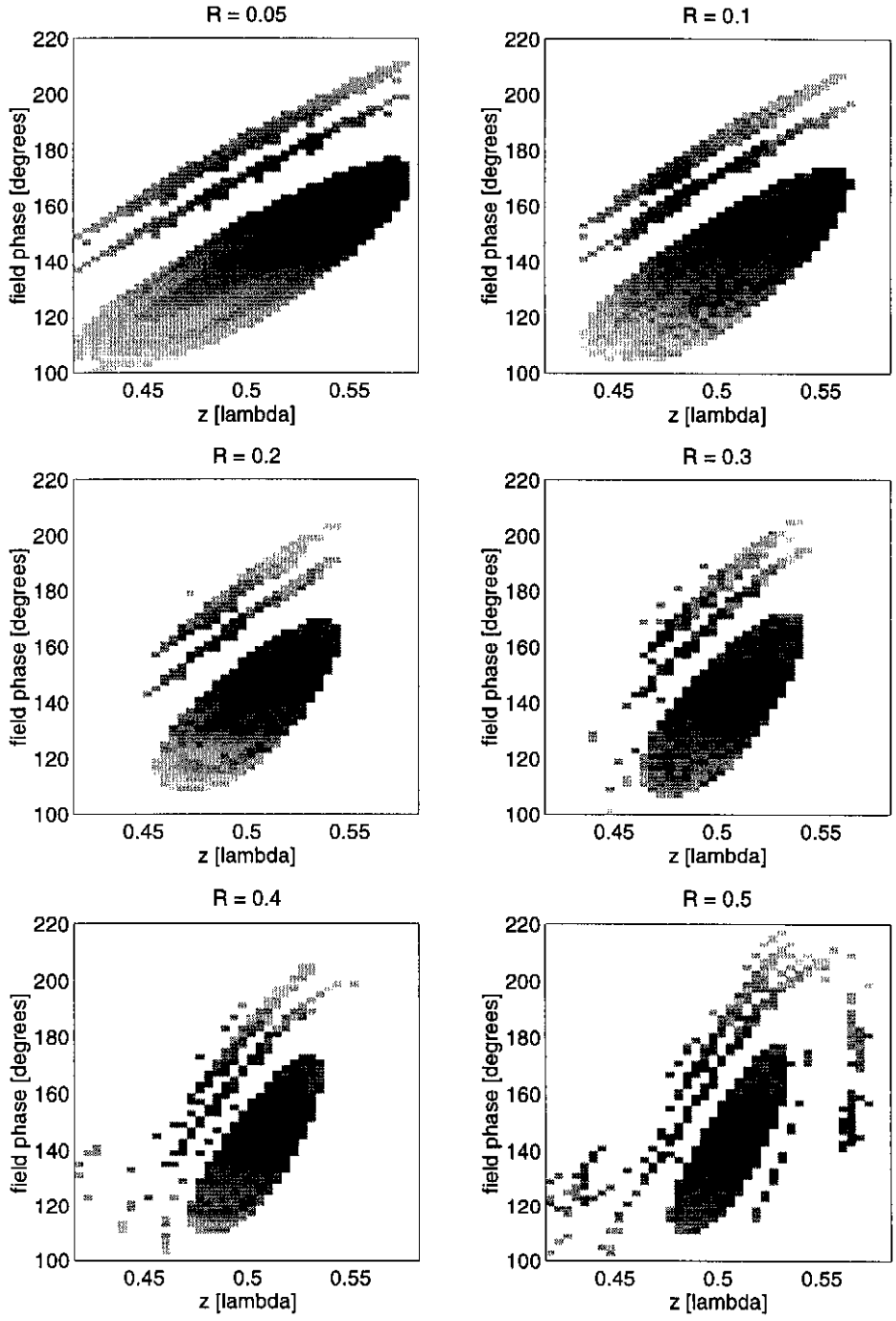

Figure 12. Distance function of the one–point MMP process of order three after 30 impacts when $R = 0.05$, 0.1, 0.2, 0.3, 0.4 and 0.5. The frames of the pictures correspond to the SW case.

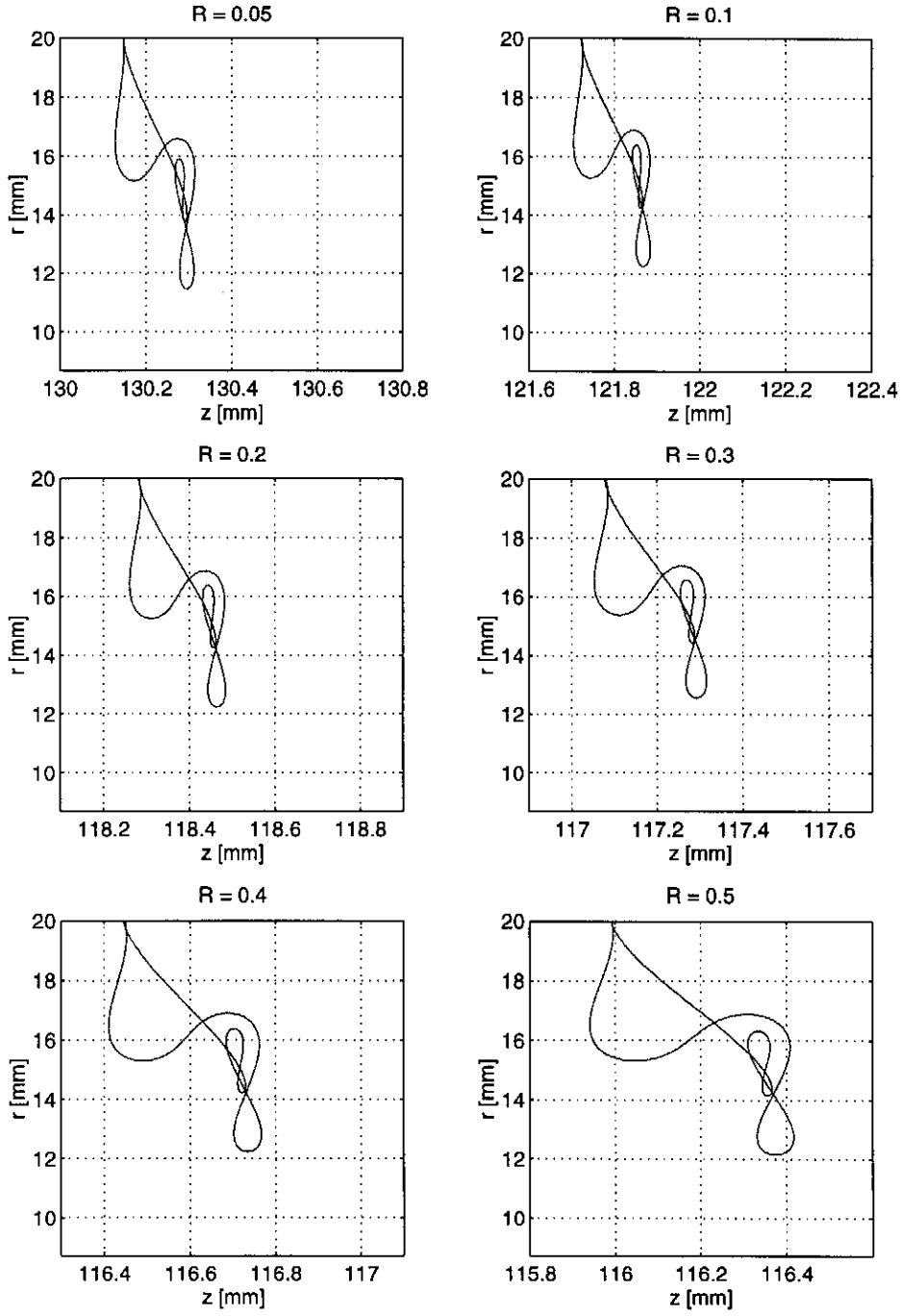

Figure 13. Electron trajectories of the one–point MMP process of order three when $R = 0.05$, 0.1, 0.2, 0.3, 0.4 and 0.5. The upper and lower borders of the pictures correspond to the outer and inner conductors of the line. Note that the trajectories are again predominantly radial.

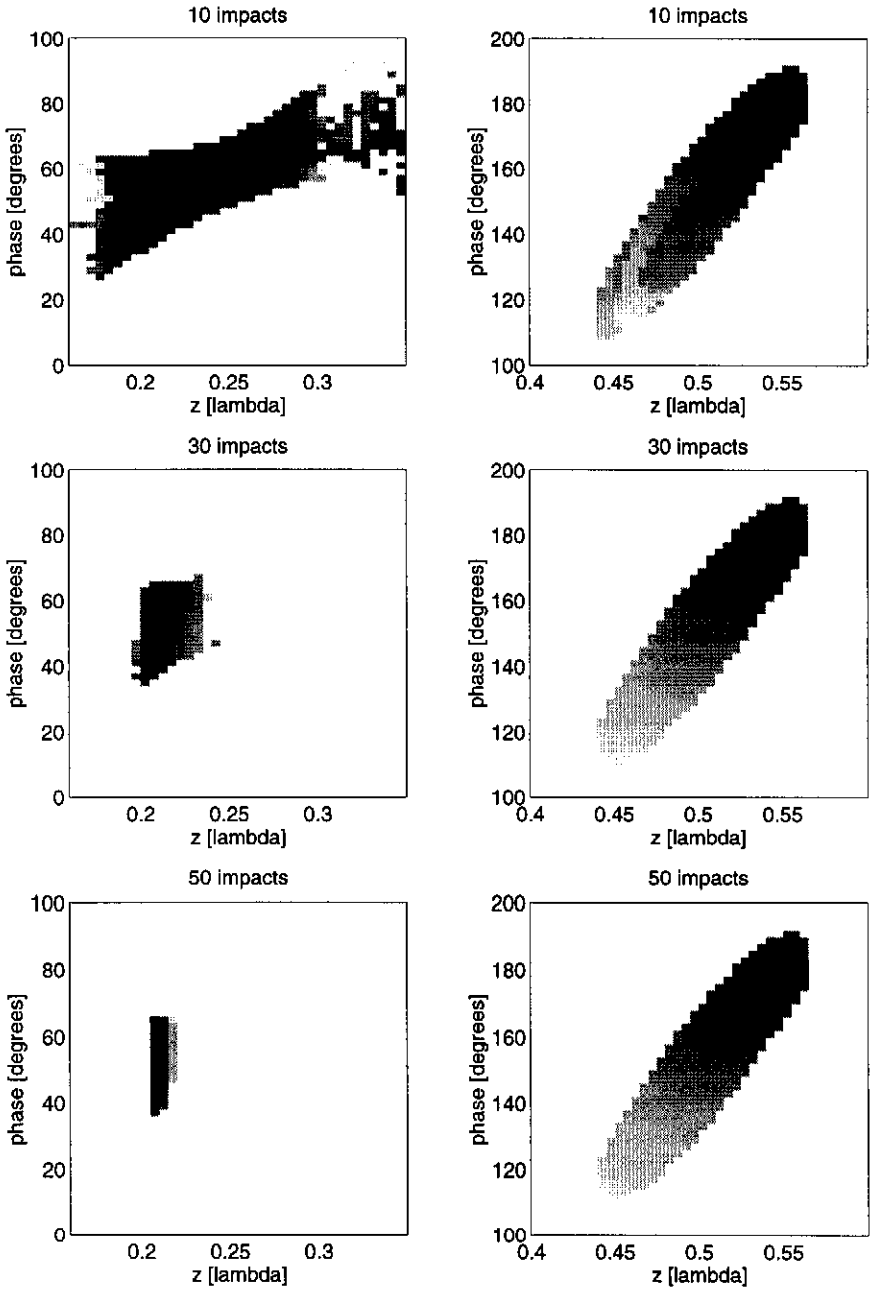

Figure 14. Distance functions after 10, 30 and 50 impacts due to the one-point EMP and MMP processes of order one when $R = 0.25$. On the left hand side are the EMP process and on the right hand side are the MMP process, respectively. The frames of the pictures correspond to the SW case.

heuristical explanation to this phenomenon is the following. Close to the maximum of the SW magnetic field, the SW and TW parts of the field drive electrons to the opposite directions, but the total field drives electrons towards the fixed point, yielding to an attractive fixed point.

Figure 15 displays the trajectories due to the EMP (the top frame) and MMP (the bottom frame) one–point processes of order one when $R = 0.25$. In the middle of the pictures are the stationary trajectories initiated close to the fixed points, (marked by circles), and on the left the initial points (marked by asterisks) are moved 1 mm to the left and on the right initial points are moved 1 mm to the right, respectively. In the EMP case the electrons start to drift away from the fixed point, whereas in the MMP case they start to drift towards it!

Summarizing, the EMP processes are *attractive* in the phase direction but *repelling* in the spatial direction. In other words, all electrons outside the fixed point in the axial direction are slowly drifting to the shadow set. The (electric) MP in the SW operation was found to behave similarly [2]. The MMP processes turn out to be *attractive* in both directions. In other words, electron trajectories starting from a certain phase space neighborhood of the fixed point drift toward the fixed point. Therefore, the MMP processes are not so sensitive to the perturbations of the field than the corresponding EMP processes are. However, when R is very small, both processes resemble TW MP. Then the traveling of the MP electrons is a dominant property.

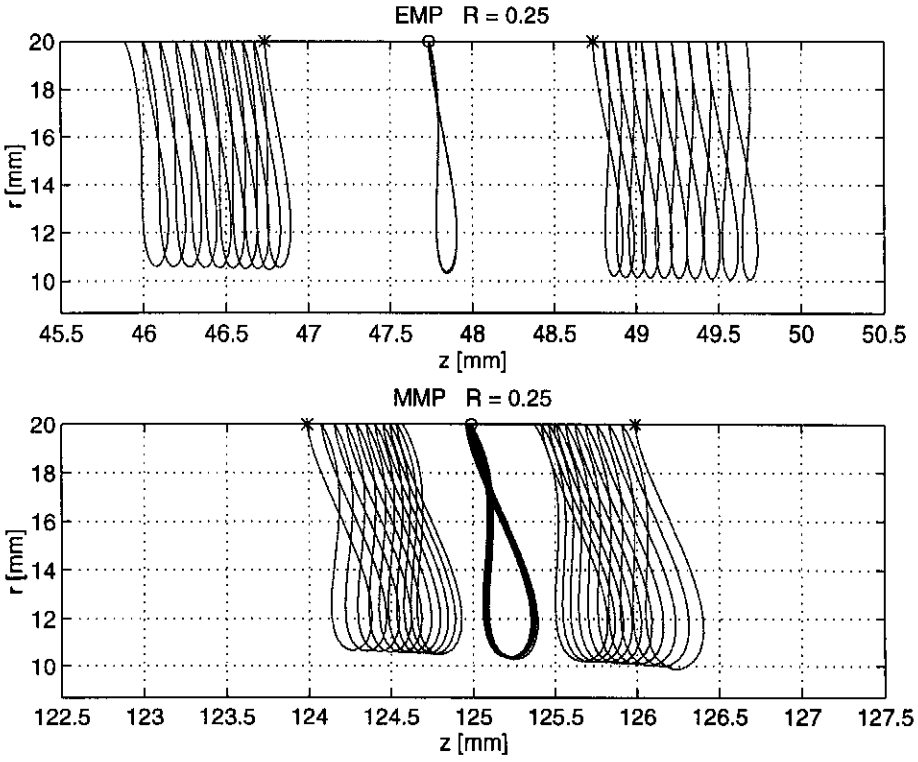

Figure 15. Electron trajectories of the one–point EMP and MMP processes of order one when $R = 0.25$. The fixed point, denoted by a circle, is repelling in the axial direction in the EMP case but attractive in the MMP case. In both cases the fixed point is attractive in the phase direction.

5 Scaling laws

Our previously found scaling laws (3) for the MP power levels, are found to be valid in the MW and TW cases too, for both the EMP and MMP processes. In particular, the MP bands of Figure 9 (and Figure 16) remain the same and they scale according to the scaling laws (3) when the diameter, impedance and frequency are altered.

6 Summary

In this report we have analyzed electron multipacting in coaxial lines when the wave is either a pure one–way traveling wave (TW) or a mixed wave. When the wave is a purely one–way traveling one the structure of MP power levels resembles the standing wave (SW) case. Similar MP processes can be recognized in both the SW and TW cases, even the secondary yields are of the same size. In the TW case the MP power levels appear at four times higher power values than the corresponding levels in the SW case. Furthermore, in the TW operation the wall impacts of the MP electrons appear again close to the maximum of the electric field and, furthermore, the electrons are slowly traveling along with the wave as the wave form moves. Due to this traveling in the TW operation MP may occur on the entire line and MP is of mixed nature, i.e., MP is due to both the electric and magnetic fields.

When the wave is neither purely one–way traveling nor perfectly reflected, the MP structure is more complicated. In that case we are able to recognize two families of MP of different nature. One appears close to the maximum of the SW electric field and can be identified as electric multipacting (EMP); another appears close to the maximum of the SW magnetic field and is called the (coaxial) *magnetic multipacting* (MMP). Further, in the MW operation MP is found to be related to certain fixed points in the phase space. In the case of EMP the fixed point is repelling in the spatial direction but attractive in the phase directions, whereas the MMP is attractive in both directions.

When the wave is switched from SW to TW, and vice versa, we have found a simple scaling law for the EMP power bands with respect to the reflection coefficient R, $0 \leq R \leq 1$. For the other bands, the MMP bands, however, we have not found any simple scaling law. Furthermore, the scaling laws (3) with respect to the diameter, impedance and frequency are found to be valid in the MW and TW cases, too.

Figure 16 gives a simplification of Figure 9 and summarizes the MP power bands in the MW operation. The 10 first MP power bands are shown as functions of the incident power and the reflection coefficient. The dark bands correspond to such processes where the average impact energy is in the range 400 eV - 1500 eV, i.e., the secondary yield is greater than one. The band at the right–most corresponds to a first order process. When moving to the left the order increases. The right–most and left–most processes, i.e., the processes of order one and 10, are plotted by dashed lines because the secondary yield is less than one (in this particular geometry).

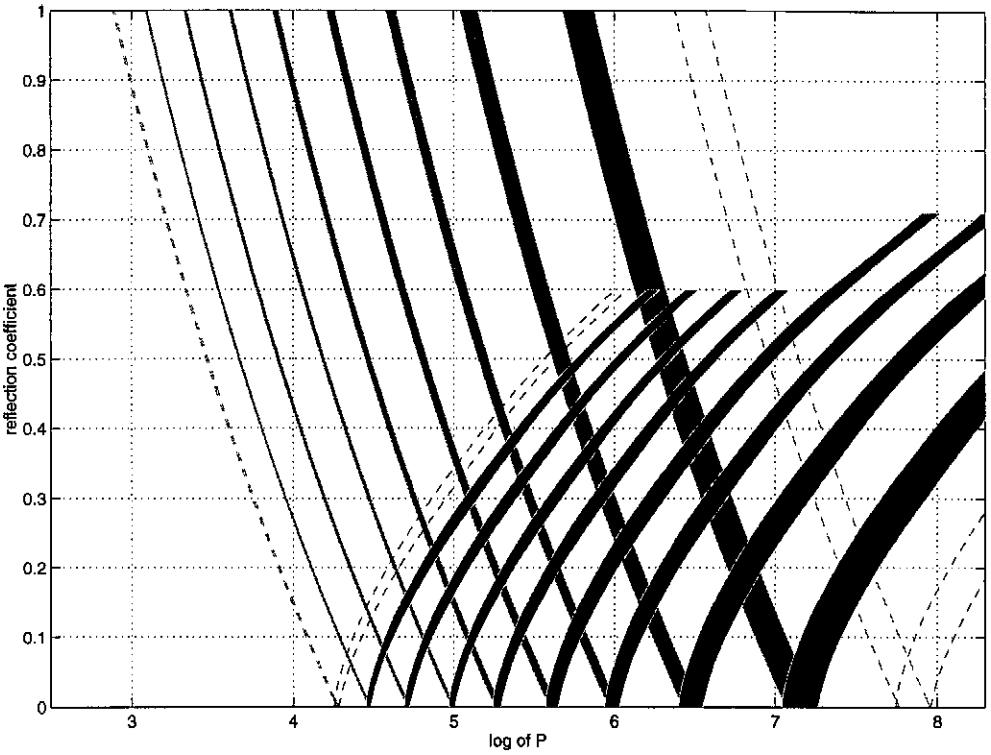

Figure 16. The MP power bands when the wave is switched from SW to TW and vice versa. The horizontal axis gives the natural logarithmic of the incident power (in kW). The bands due to the higher order MMP processes stop at $R = 0.6$, because the MMP bands are hard to identify when R is close to one.

Acknowledgments

The computations presented in this report were carried out in the joint project of Rolf Nevanlinna Institute, University of Helsinki, Finland, and Deutsches Elektronen–Synchrotron DESY, Hamburg, Germany. The author wish to thank Dr. Dieter Proch and Jacek Sekutowicz for a very good and fruitful co–operation. Also Prof. Jukka Sarvas and MSc Hannu Mäkiö are highly acknowledged for numerous enlightening discussions. I also thank Prof. Erkki Somersalo for his valuable suggestions and comments during the work.

References

[1] Piel, H.: Superconducting cavities. In: *Proceedings of the CERN Accelerator School: Superconductivity in Particle Accelerators*, Geneva 1989, 149–196

[2] E. Somersalo, P. Ylä–Oijala and D. Proch: Electron Multipacting in RF Structures. TESLA Reports 14–94.

[3] E. Somersalo, P. Ylä–Oijala and D. Proch: Analysis of Multipacting in Coaxial Lines. IEEE Proceedings, PAC 95, pp. 1500–1502.

[4] E. Somersalo, P. Ylä–Oijala, D. Proch and J. Sarvas: Computational Methods for Analyzing Electron Multipacting in RF Structures. To be submitted to *Particle Accelerators*.